Noname manuscript No.
(will be inserted by the editor)

Myriapod-like ambulation of a segmented microrobot

Katie L. Hoffman · Robert J. Wood

Received: date / Accepted: date

Abstract Segmented myriapod-like bodies may offer performance benefits over more common fixed body morphologies for ambulation. Here, the design of a segmented ambulatory microrobot with a flexible backbone is presented. A dynamic model describing the motion of the microrobot is used to determine body parameters. A three-segment microrobot was fabricated using the Smart Composite Microstructures process and piezoelectric bimorph actuators, and forward locomotion on a flat surface was demonstrated. The footprint of the 750 mg microrobot is 3.5 by 3.5 cm, and it has potential advantages over rigid body hexapedal microrobots in climbing, versatility, and stability.

Keywords Microrobots · Biomimicry · Ambulatory Robots · Modular Robots

1 INTRODUCTION

Advances in microfabrication techniques and an improved understanding of the locomotory mechanisms of insects have enabled recent success in the development of ambulatory microrobots. Examples of successful combinations of biological inspiration and layered composite manufacturing are RoACH, a 2.4 g autonomous hexapod robot capable of speeds up to one body length per second (Hoover et al. 2008), DASH, an autonomous robot modeled after a cockroach robust enough to withstand falls at 10 m/s and larger at about 10 cm in length (Birkmeyer et al. 2009), and HAMR, a microrobot that has demonstrated forward locomotion and weighs only 90 mg (Baisch and Wood 2009). Each of these robots was created using the Smart Composite Microstructures (SCM) method of fabrication (Wood et al 2008). Additionally, they were all modeled after cockroaches, utilize the alternating tripod gait seen in insects, and have a central body that houses electronics and actuators and use six comparably massless legs.

An alternative to fixed bodies and hexapod morphologies is to use a segmented body with flexibility in the backbone that allows relative motion between segments, similar to myriapods. A study of myriapods indicates that segmented, many-legged robots may have advantages over more traditional morphologies, including:

1. Speed: While cockroaches and other rigid-body hexapods can achieve maximum speeds of 40-50 body lengths/second (Full and Tu 1991), the fastest recorded speed of centipedes is slightly less at around 10 body lengths/second (Manton and Harding 1952); however, centipedes are still agile creatures, able to catch live prey, including cockroaches and other similarly sized or even larger insects and mammals. In addition to utilizing body undulations to amplify step size, the flexibility inherent in the bodies of centipedes allows them to morph to surfaces, easily turn, and transition between horizontal and vertical surfaces. This has the potential to make centipede microrobots faster than similarly sized rigid body hexapod robots on rough terrain and when changing direction.

2. Stability: The large number of legs characteristic to centipedes, up to 191 in some species of myriapods (Edgecombe and Giribet 2006), allows for a variety of gaits and added stability. In many cases, centipedes form a tripod by grouping legs together into clumps

K.L. Hoffman
Harvard University
Tel.: +1 617 384-7892
Fax: +1 617 384-7892
E-mail: khoffman@fas.harvard.edu

R.J. Wood
rjwood@eecs.harvard.edu

(Full and Tu 1991). With many legs distributed along the length of the body, the center of mass is likely to remain within the triangle of support, allowing for static stability.

3. Robustness: Studies involving the removal of different numbers of legs from centipedes were performed with insignificant changes in locomotory capabilities, including gait, speed, and stability, suggesting a multi-segment robot could be robust to failures (Manton and Harding 1952).

4. Climbing and agility: The number of attachment points increases linearly with the number of segments of the centipede or robot, and the flexibility in the body allows centipedes to curl around ledges and move from horizontal to vertical surfaces without drastic gait changes.

5. Versatility and adaptability: The modular design of a segmented centipede robot would enable adding and removing segments to better perform different tasks.

While a centipede robot could have many benefits, there are challenges with creating such a device. Due to the use of flexures and linear actuators for devices at this scale, the design of locomotory mechanisms and interconnections between segments differs from larger-scale devices. An underlying question regarding centipede locomotion relates to muscle actuation in terms of body undulations. Manton concluded that the body undulations were passive (Manton and Harding 1952). More recent work involving electromyograms attached to the lateral flexor muscles of centipedes found that muscles actively promote body undulations (Full and Tu 1991). The design and modeling of this type of microrobot could answer open questions pertaining to effective ambulation at small scales, including the optimal method of introducing flexibility, efficient actuator placement, and the appropriate number of legs. Microfabrication processes, including the SCM process, have enabled the creation of micron-scale features, but these tend to have low yield and require multiple manual assembly steps. A segmented microrobot would require batch fabrication techniques and automated assembly to increase yield. By developing batch fabrication methods and making many of the same components in parallel, the fabrication time for a segmented microrobot may not increase significantly with an increase in number of legs.

Dynamic models of segmented robots are also very rare. It is often straightforward to model the dynamics of individual segments, but fairly challenging to accurately describe the interactions between segments and with the environment. On the micro-scale, the dynamics for robots with relatively rigid bodies and massless legs, similar to cockroaches, have been modeled. Videos and force data from actual cockroaches have been used to create a dynamic model of cockroach locomotion which can be extended to similar cockroach-style microrobots to predict their motion and provide a design guide (Holmes et al. 2006). Unfortunately, this model does not encompass locomotion of microrobots with flexible segmented backbones. The dynamics of larger segmented robots, such as a salamader robot (Jimenez and Ikspeert 2007, Matthey et al 2008) and a segmented, legged robot demonstrating different undulatory modes (Sfakiotakis and Tsakiris 2009), and controllers for these robots were studied. Simulations were also performed to find an optimal number of legs for larger segmented robots(Nohara and Nishizawa 2005). These dynamic models created for larger segmented robots do not accurately describe locomotion of microrobots due to scaling effects and actuation and fabrication differences. To properly answer questions associated with control and design of segmented ambulatory microrobots, a dynamic model is necessary.

An initial design for a multi-segment ambulatory microrobot was presented (Hoffman and Wood 2010). The motion of a suspended segment was verified by comparison with a kinematic model. While the individual segment displayed motion as predicted by the model, the notional design was difficult to fabricate, had a high center of mass and awkward actuator placement, exhibited a singularity in the backbone, and was based on a kinematic model, neglecting the dynamics of the system and individual segments. Wiring was also done by hand, which was time consuming and unreliable. Regardless, the segment concept was successful and showed promise for creating segmented robots.

Many of the challenges associated with segmented microrobots are addressed here. A detailed dynamic model for a multi-segment, flexible ambulatory microrobot was created and simulated in Sect. 3. This model was then used to find appropriate parameters relating to a novel compact and modular notional design described in Sect. 2. The SCM process and some additional fabrication techniques necessary for constructing a microrobot with many repeated segments was used to create the chosen design in Sect. 4. The finished robot, measuring 3.5 by 3.5 by 1 cm and weighing 750 mg, demonstrated stable forward locomotion on a horizontal surface as shown in Sect. 5. This microrobot may soon be used as a platform for distributed robotics, inspire batch fabrication techniques, advance control technology for ambulatory microrobots, enhance climbing capabilities of microrobots, and provide a microrobot to assist in search and rescue missions, hazardous environment exploration, and surveillance. The dynamic model can also be used as a design guide for model-

ing of other segmented robots and inspire research and modeling of actual myriapods and other species with segmented or compliant bodies.

2 NOTIONAL DESIGN

The design of a segmented robot can be described on two levels; each individual segment and how these segments interact. Generally speaking, each segment and the connections between adjacent segments should have sufficient degrees of freedom (DOF) to allow segments to move relative to each other and create global locomotion. In this design, each segment has one actuated degree of freedom in the horizontal plane, generating a torque at the shoulder, and one actuated DOF in the vertical plane, which allows legs to be lifted and placed on the ground. An additional DOF in the horizontal plane is passive and allows the foot to pivot with respect to the ground. To achieve forward motion, a segment places one foot on the ground, defined as the stance foot, while lifting the opposite foot, or the swing foot. The segment then rotates about the stance foot by applying a torque at the shoulder, elevates the previous stance foot while lowering the previous swing foot, and rotates about the new stance foot. This process is repeated for subsequent steps. These rotating and stepping motions, in the horizontal and vertical planes respectively, are caused by two dual piezoelectric bimorph cantilever actuators oriented perpendicular to one another. Additional motors, such as Squiggle motors (New Scale Technologies) and shape memory alloy (SMA) were considered for this robot. DC motors at small scales tend to have very low power densities due to their use of rotating components which suffer from the enhanced deleterious effects of friction at this scale. SMA actuators have a significantly lower bandwidth than peizoelectric actuators, which would limit the stepping frequency of the microrobot. Piezoelectric actuation has previously been shown to be successful for locomotion at this scale (Lobontiu et al. 2001 and Sahai et al. 2006), and was determined to be the best option for this microrobot. The actuator placed parallel to the horizontal plane lifts each leg, while the actuator situated perpendicular to the horizontal plane rotates the segment about the stance foot. The tips of each dual cantilever actuator are attached to four-bar mechanisms fabricated using the Smart Composite Microstructures process (Wood et al. 2008) described in Sect. 4. This results in four four-bar mechanisms per segment. The four-bar mechanisms convert the actuator force into a torque, or when no load is applied, a linear actuator tip displacement into a rotational motion. This is illustrated in Fig. 1. The horizontal plane motion and stance control four-bars for each leg are attached perpendicularly to create a mechanism that produces a smooth elliptical motion. There are two of these mechanisms per segment, one at each shoulder joint (Fig. 2). The segmented nature of the microrobot and relative motion between segments does not allow the actuators to be grounded to a central body as in other ambulatory microrobots (Baisch and Wood 2009 and Hoover et al. 2008), requiring the novel design presented here.

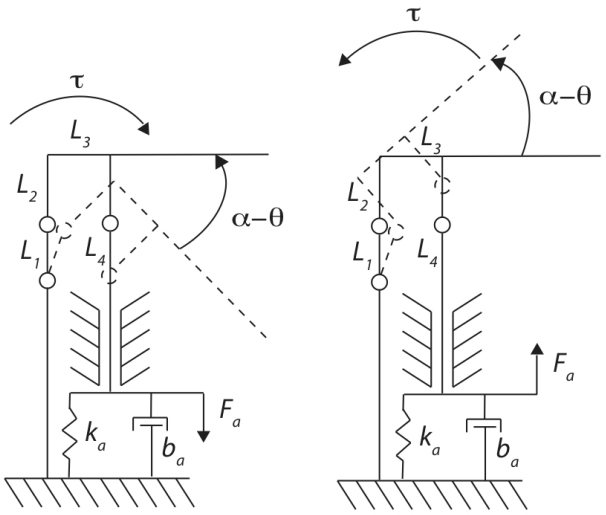

Fig. 1 Diagram showing how actuator force is mapped to a torque using a four-bar mechanism. Dotted lines indicate rotation of four-bar mechanism.

Each dual cantilever actuator has an electrical ground, a bias voltage, and one drive signal. With two dual cantilever actuators per segment, one for stance control and one for rotating the segment about the stance foot, two drive signals are required. The two dual cantilever actuators share common ground and bias signals. The two sides of each dual cantilever actuator are oppositely poled, as indicated in the wiring diagram in Fig. 3(a-b). This means that by using only one drive signal per dual cantilever actuator, one leg will be elevated while the opposite leg is placed on the ground. Additionally, the opposite poling of the dual cantilever actuator that controls the segment rotation will allow the segment to pivot about the stance foot while reseting the opposite leg in preparation for the next step. The result of this opposite poling is shown in Fig. 3(c) with a plot of the normalized deflection of each side of a dual cantilever actuator as a function of the normalized drive signal.

Multiple segments are connected with a flexible backbone to form the segmented microrobot. The backbone is a continuous structure composed of sarrus linkages and flexures and spans the length of the microrobot,

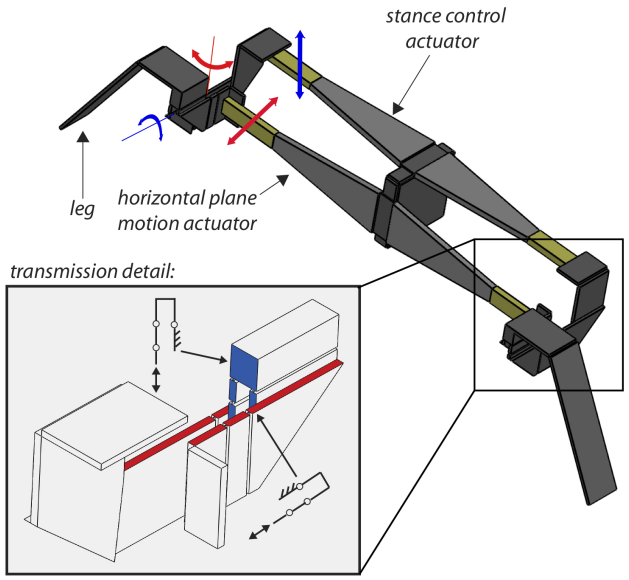

Fig. 2 Solid model of an individual segment showing motion of stance control actuator and associated four-bar in blue and horizontal plane motion actuator and associated four-bar in red.

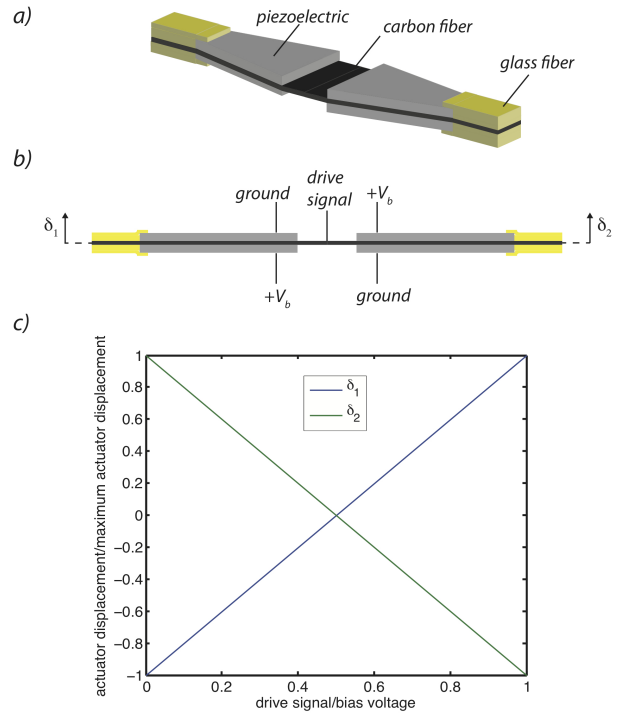

Fig. 3 A a) three-dimensional rendering of a dual cantilever actuator pair with a b) wiring diagram showing the opposite poling of both sides of the actuator and a c) plot showing both normalized actuator tip displacements with drive signal normalized to maximum bias voltage.

attaching to the top of each segment at the base of the actuators. The design of the backbone can include any number of prismatic and rotational joints and springs. Here, a configuration which results in 2 DOF per segment is used. Two flexures, which act like torsional springs, and the sarrus linkage, which compresses and extends linearly, separate each segment. The sarrus linkage reinforces the backbone by decreasing the possibility of off-axis rotations while still allowing the backbone to compress and extend. The flexures in the sarrus linkage are initially bent at some equilibrium angle to allow both extension and compression of the sarrus linkage and, therefore, both positive and negative restoring forces on adjacent segments when considering the body dynamics. The direction of compression of a sarrus linkage and axes of rotation of adjacent flexures is depicted in Fig. 4, and a solid model of an assembled three segment robot with integrated backbone is shown in Fig. 5. Three segments were chosen for this design to allow the implementation of the alternating tripod gait while still maintaining static stability; however, the work here can easily be used to create a microrobot with many segments.

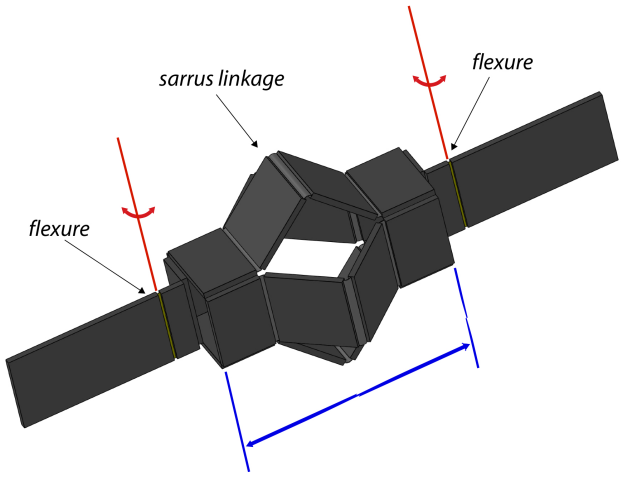

Fig. 4 Backbone interconnections showing segment attachment points, axes of rotation of flexures in red, and direction of compression of sarrus linkage in blue.

3 DYNAMIC MODEL

While kinematics guided the initial design of the multi-segment microrobot (Hoffman and Wood 2010), to predict the torques necessary for stable forward locomotion, a dynamic model is necessary. The underactuated

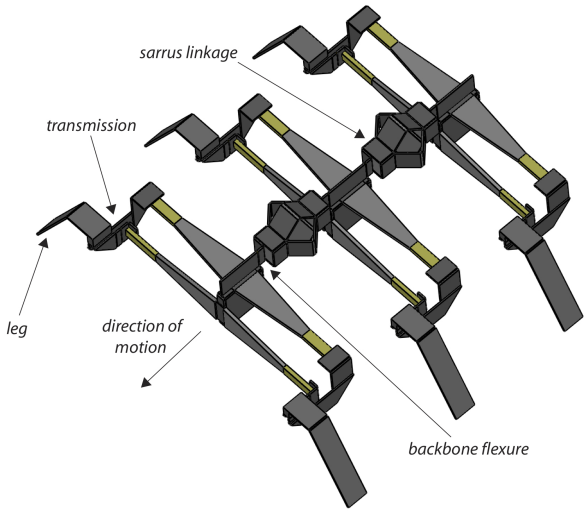

Fig. 5 Rendering of a three segment centipede robot illustrating key components.

design also makes a kinematic model insufficient to accurately describe the motion. A detailed dynamic model of the system can be used to not only predict the combined effects of the actuator and body dynamics but also be used to determine reasonable body parameters and control schemes, according to the desired performance of the robot as measured by an appropriate cost function.

To predict motion, a dynamic model was constructed for a multi-segment robot with the notional design described in Sec. 2. To fully describe the dynamics of the system, it is necessary to consider the dynamics associated with each individual segment and the interactions between adjacent segments.

The modeling of microrobots fabricated using the SCM process, which utilizes short flexures as opposed to pin joints and linear actuators rather than fully rotational motors, differs from the modeling of macroscale robots. A diagram illustrating the overall body kinematics in the horizontal plane is shown in Fig. 6. The horizontal plane motion is assumed to be decoupled from the vertical plane, or leg lifting, motion. The stance control is related to the horizontal plane motion as a simple binary input, dictating the stance and swing feet for each segment, and is assumed to be instantaneous. Each segment has two DOF in the horizontal plane. These are the rotation of the leg, α_i, and the rotation of the body, θ_i, with respect to an axis perpendicular to the direction of motion of the robot. The foot is allowed to rotate with respect to the ground, but not translate. The mass, m, of each segment is concentrated in the body, which has an associated inertia, I. The legs and backbone are assumed to be massless. The robot is underactuated and the input torque, τ_i, is applied at the shoulder joint. The backbone's two rotational and one linear joint allow each segment to move relative to adjacent segments. The segments are numbered in increasing order in the direction of motion, beginning with the most anterior segment. Sets of intersegmental joints are also numbered in increasing order beginning with the joints located between the most anterior two segments. The important geometric body parameters are the leg length, L_{leg}, defined as the horizontal distance between the foot and the shoulder, the body length, L_b, defined as half the length of a segment in the direction of motion or the distance between the middle of the segment and the adjacent flexure, the body width, w_b, or distance from shoulder to center of mass for each segment, and the equilibrium length of the sarrus linkage, l_e. The pivot point for each foot is labeled as (x_i, y_i). Additionally, $c_{f,i} \in [-1, 1]$, is used to describe which foot is the stance foot for each segment. For each segment, there are 4 state variables: the leg and body rotation and angular velocities.

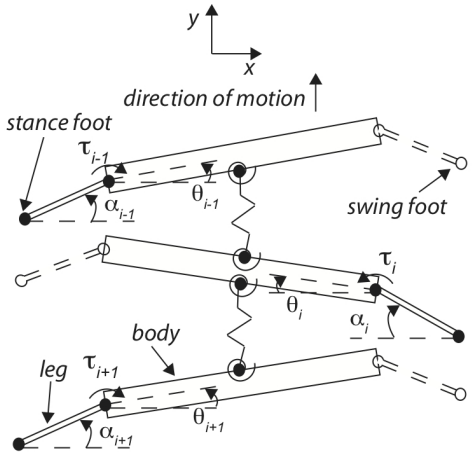

Fig. 6 Depiction of horizontal plane motion of a three segment microrobot.

The Euler-Lagrange method was used to formulate the equations of motion for this system. The energies of the system are written out in a modular fashion to be applied to a microrobot with any number of segments. Since the mass and body inertia is concentrated in the body of each segment, the kinetic energy can be calculated by

$$KE = \frac{1}{2}\sum_{i=1}^{n} I_{cm}\dot{\theta_i}^2 + m(\dot{x_i}^2 + \dot{y_i}^2) \tag{1}$$

where I_{cm} is the segment inertia about the center of mass, m is the segment mass, and $\dot{x_i}$ and $\dot{y_i}$ are the forward and lateral velocities at the center of mass. The

kinetic energy can be written in terms of the state variables by replacing the linear velocities with functions of the leg and body angles and angular velocities, according to the following relations

$$\dot{x}_i = -c_{f,i} L_{leg} \dot{\alpha}_i \sin\alpha_i + c_{f,i} w_b \dot{\theta}_i \sin\theta_i \tag{2}$$

and

$$\dot{y}_i = L_{leg} \dot{\alpha}_i \cos\alpha_i + w_b \dot{\theta}_i \cos\theta_i \tag{3}$$

The kinetic energy associated with the actuator motion mapped through the four-bar mechanism is negligible compared to the other system energies and is excluded from the calculations.

The potential energy for the system includes only that stored in each of the spring elements. The potential energy stored in the flexures of the four-bar mechanism is negligible as a result of the small amount of rotation of these flexures. Due to the nature of the fabrication and the flexures used to create rotational joints, the rotational and linear backbone joints are modeled as torsional and linear springs using the Pseudo Rigid Body approximation. The energy associated with these springs is given by

$$PE_s = \frac{1}{2}\sum_{i=1}^{n-1} k_l \Delta l_i{}^2 + k_t(\gamma_{a,i}^2 + \gamma_{p,i}^2) \tag{4}$$

where k_l is the spring constant for the sarrus linkage, assumed to be linear, k_t is the torsional spring constant of the backbone rotational joints, Δl_i is the sarrus linkage compression, related to the state variables as

$$\Delta l_i = S_i - l_{eq} \tag{5}$$

where l_{eq} is the equilibrium length of the sarrus linkage and

$$S_i = \sqrt{(x_{p,i} - x_{a,i+1})^2 + (y_{p,i} - y_{a,i+1})^2} \tag{6}$$

γ_a and γ_p are the rotational spring angles anterior and posterior to each segment, respectively. These can be written in terms of the state variables as

$$\gamma_{a,i} = c_{f,i}\theta_i + sin^{-1}\frac{x_{p,i-1} - x_{a,i}}{S_i} \tag{7}$$

$$\gamma_{p,i} = c_{f,i}\theta_i - sin^{-1}\frac{x_{a,i+1} - x_{p,i}}{S_i} \tag{8}$$

$x_{a,i}$, $y_{a,i}$, $x_{p,i}$, and $y_{p,i}$ are the x and y coordinates of the flexures anterior and posterior to each segment, respectively. These can be written in terms of the state variables associated with adjacent segments, but are not shown here for brevity.

Another source of energy storage is the piezoelectric actuator. The actuator can be modeled as a spring, k_a, and damper, b_a, in parallel with a force source. The deflection of the actuator is directly related to the state variables via the linearized transmission ratio, $T_h = \frac{1}{L_{3,h}}$, where $L_{3,h}$ is the third link in the transmission, shown in Fig. 1. The potential energy of the actuator is given by

$$PE_a = \frac{1}{2}\sum_{i=1}^{n} k_a \frac{1}{T_h^2}(\alpha_i - \theta_i)^2 \tag{9}$$

In addition to the kinetic and potential energy of the system, the external energy transfer can be written in terms of the losses due to friction at the foot pivot point and damping from the actuator and the energy input associated with the torque supplied by the actuator. The flexure damping is assumed to be negligible as shown by a similar device in (Steltz et al 2006). The work is given by

$$W = \sum_{i=1}^{n} \tau_i(\alpha_i - \theta_i) - b_a \frac{1}{T_h^2}(\alpha_i - \theta_i)(\dot{\alpha}_i - \dot{\theta}_i) - \tau_f \alpha_i \tag{10}$$

τ_i is the input torque from the actuator, ignoring the state dependency of the actuator, which is more conveniently reflected through the use of an actuator spring constant. τ_i can be calculated using the actuator force and transmission ratio. b_a is the actuator damping coefficient, and τ_f is the friction due to the rotation of the foot with respect to ground.

The Lagrangian can be written in terms of these energies as

$$L = KE - PE_a - PE_s \tag{11}$$

and the Euler-Lagrange method of formulating differential equations can be used to find the equations of motion according to

$$\frac{\delta L}{\delta q_i} - \frac{d}{dt}\frac{\delta L}{\delta \dot{q}_i} = -\frac{\delta W}{\delta q_i} \tag{12}$$

The resulting differential equations can be solved numerically as described below.

Supplementary to the equations describing the motion of the microrobot during each step, are the transitions between stance and swing feet. Collisions between swing legs and ground are modeled as inelastic and instantaneous. The method for modeling collisions of multi-link systems was taken from (Chen and Tedrake 2007). Using the idea of conservation of momentum for both the leg and body around the foot and the body about the shoulder joint gives two equations with two unknowns. Due to the massless leg, this reduces to conservation of the linear velocity at the center of mass. Writing this in terms of the state variables, however, leads to step changes in the leg and body angular velocities due to differences in the liftoff and touchdown angle of the leg. This difference is due to the unique

coupling between the two legs of each segment. Using the same drive signal to control the motion of each leg in the horizontal plane causes a torque to be applied at the shoulder connected to the stance foot while a displacement is prescribed to the shoulder attached to the swing foot. This is a result of the leg being massless, causing no load on the swing foot, allowing it to rotate freely.

The body and leg angular velocities post-collision are given by

$$\dot{\alpha_i}^+ = \frac{-\dot{\alpha_i}^-}{1 - \frac{\sin\theta_i^+ \cos\alpha_i^+}{\sin\alpha_i^+ \cos\theta_i^+}} \left[\frac{\sin\theta_i^+ \cos\alpha_i^-}{\sin\alpha_i^+ \cos\theta_i^+} + \frac{\sin\alpha_i^-}{\sin\alpha_i^+} \right] \quad (13)$$

and

$$\dot{\theta_i}^+ = \frac{-L_{leg}\cos\alpha_i^+}{w_b \cos\theta_i^+}\dot{\alpha_i}^+ + L_{leg}\frac{\cos\alpha_i^-}{w_b\cos\theta_i^+}\dot{\alpha_i^-} + \frac{\cos\theta_i^-}{\cos\theta_i^+}\dot{\theta_i^-} \quad (14)$$

α_i^+ is the leg touchdown angle, which is given by

$$\alpha_i^+ = -(\theta_i^- + \beta_{max}) \quad (15)$$

where β_{max} is the amount of rotation of the swing leg due to the coupling between the stance and swing leg and can be calculated using kinematics with

$$\beta_{max} = \delta_{max} T_h \quad (16)$$

where δ_{max} is the maximum deflection of the actuator calculated using equations in (Wood et al. 2005).

The nonlinear and hybrid-dynamic nature of the system makes it impossible to find an analytical solution for the differential equation describing the motion of the system. Instead, the motion is simulated using Matlab and a numerical differential equation solver, ode45. The simulation predicts the motion of the robot, plots relevant variables, such as the angle of rotation and angular velocity for each segment, the system energy, and the flexure bending angles and sarrus linkage compression, and animates the motion. The parameters necessary for the simulation are given in Tab. I. These are based on the actual three-segment microrobot described in Sect. 5.

Using these parameters and a sinusoidal drive signal at 2 Hz, as shown in Fig. 7(a), the motion of the robot was simulated for three and a half steps, starting in the neutral configuration. The drive signal for each segment is 180 degrees out of phase of adjacent segments, creating the statically-stable alternating tripod gait characteristic of hexapods, and while the drive signal shown in Fig. 7(a) looks discontinuous at feet switching times, this is merely an artifact of how the torque is defined about the stance feet. The voltage input to the actuators is continuous. The dominating

Table 1 Centipede Microrobot parameters

L_{leg} (mm)	10
L_b (mm)	3
w_b (mm)	10
l_{eq} (mm)	4
L_3 (μm)	480
k_a (N/m)	860
k_l (N/m)	2.9
k_t ($\mu Nm/rad$)	7.6
$\tau_{i,max}$ (μNm)	41.4
τ_f (μNm)	1×10^{-2}
b_a (Ns/m)	4.3
m (mg)	250
I (mgm^2)	9.3×10^{-3}

energy terms are shown in Fig. 7 and include the kinetic energy (Fig. 7(b)), actuator potential energy (Fig. 7(c)), and torsional spring energy (Fig. 7(d)). The remaining energy terms are on the order of $10^{-10}J$ and have less of an effect on the motion of the robot for the alternating tripod gait shown here. For different gaits and with varying surfaces, the dominating energy terms could change. The linear backbone potential energy is much smaller than the torsional backbone potential energy due to the high stiffness of the sarrus linkage. For this particular design, there is very little spring compression, and the stiff spring acts more like a kinematic constraint than a compliant member. Frames of motion are shown in Fig. 8 for three steps. Circles indicate rotational joints, squares show the center of mass of each segment, and green lines connecting segments represent the sarrus linkages.

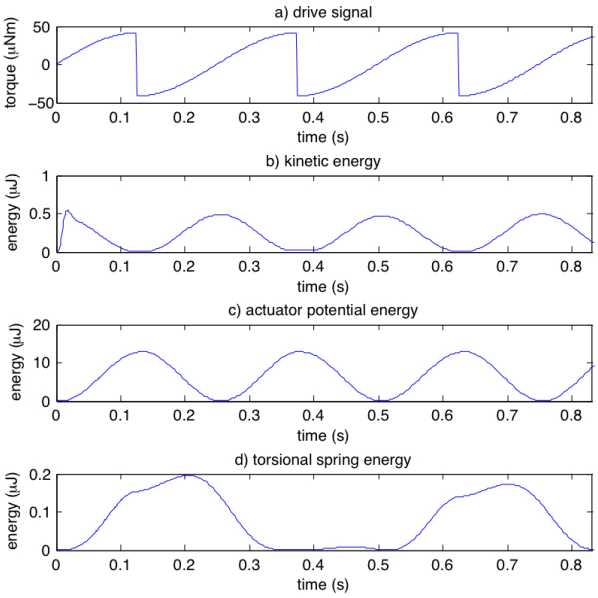

Fig. 7 (a) Drive signal with (b)-(d) dominating energy terms.

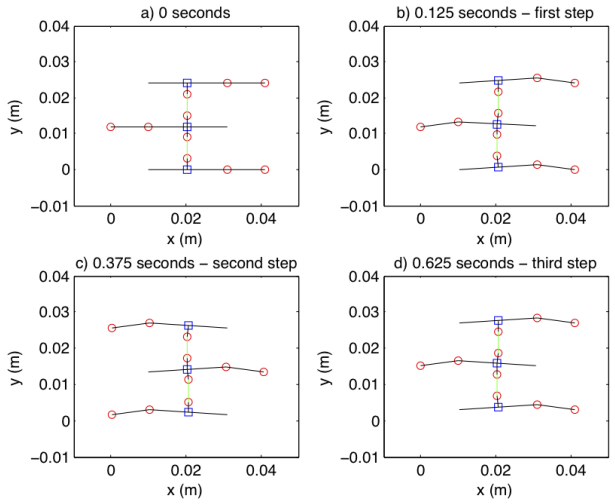

Fig. 8 Frames of motion from a simulation.

While the dynamic model only encompasses the horizontal plane and assumes decoupling from the vertical plane, it is important to include a brief description of the kinematics for the vertical plane. Using the actuator properties and equations from (Wood et al. 2005), the tip displacement from the actuators controlling the stepping mechanism can be calculated. These actuators are modeled as a displacement source to calculate the approximate angle of swing of the leg η_i using kinematics, although a more detailed and accurate model might depict them as a force source in parallel with a spring. Kinematics predict the angle of swing of the leg according to

$$\eta_i = \delta_{s,i} T_v \tag{17}$$

where $\delta_{s,i}$ is the displacement of the actuator controlling the stance and T_v is the transmission ratio for the connected four-bar mechanism, or $\frac{1}{L_{3,v}}$. The height that the leg can be lifted can be calculated using this angle and the length of the leg, $L_{leg,v}$. For the microrobot shown in Sect. 5, the leg lifting height is 2.5 mm.

4 FABRICATION

The microrobot was fabricated using the Smart Composite Microstructures (SCM) process (Wood et al. 2008). This process involves sandwiching a flexible material between a rigid laser-micromachined composite material, in this case, carbon fiber prepreg, to create a series of links separated by flexures. This is cured under vacuum to bond the layers. The 2D pattern of links and flexures can then be folded and, using an adhesive to rigidly bond some flexures at varying angles, form a 3D mechanical structure. Similarly, the piezoelectric bimorphs are made by layering the piezoelectric material, fibrous composite and glass fiber layers and are cured under vacuum (Wood et al. 2005).

Each segment consists of seven components fabricated using the SCM process: two actuators, two transmissions, two legs, and a base to mount the actuators. The backbone is made of sarrus linkages and individual flexures. Since the last step in the SCM process, or creating 3D structures out of the 2D components, is a manual process, certain techniques are used to facilitate folding, increasing yield and significantly decreasing fabrication time. This is a step towards the batch fabrication necessary to efficiently create many-legged structures. The transmission, which is two four-bar mechanisms oriented perpendicularly, is the most complex component. To create the transmission using only one component and still have the composite fibers oriented along the loading direction for each four-bar mechanism, 45 degree cut lines and 180 degree folds were used. A second technique that is used in folding the transmission is the use of three 180 degree folds to mimic two 90 degree folds. This technique is illustrated in Fig. 9. The two joints indicated in Fig. 9(a) are able to transmit force more efficiently in the neutral configuration shown in Fig. 9(b), however, this requires two difficult 90 degree folds and a small link length as shown in Fig. 9(c). To reduce issues associated with delamination, inaccurate folding, and adhesives flowing into joints that are to remain flexible, three 180 degree folds, which can be completed accurately and without difficulty are used (Fig. 9(d-f)). This makes the transmission ratio a multiple of the thickness of the composite layer (Fig. 9(g)). While, unlike the transmission, the legs only require one fold, it is at an angle that is not easy to create without a reference angle (Fig. 10(a-b)). To alleviate this issue, an additional tab machined with the desired fold angle of the leg is added to the side of the leg near the fold line. This can be folded up to meet the base of the leg and act as a template for the exact fold angle of the leg (Fig. 10(c-e)).

Another fabrication challenge is wiring as discrete wires tend to be unreliable and time-consuming to implement and could interfere with the motion of the resulting microrobot. Flex circuits have been designed, fabricated, and cured to the actuators to automate the process for internally wiring each segment. They are created using a lithography process to remove copper from a flexible copper-clad polymer sheet. The exposure step is done using a Diode-Pumped Solid-State (DPSS) laser. The flex circuits are layered between the actuators and small squares cut from a composite embedded with epoxy are placed on the reverse side of the flex circutis. This layup of actuators, flex circuits, and composite prepreg is cured under pressure, and the com-

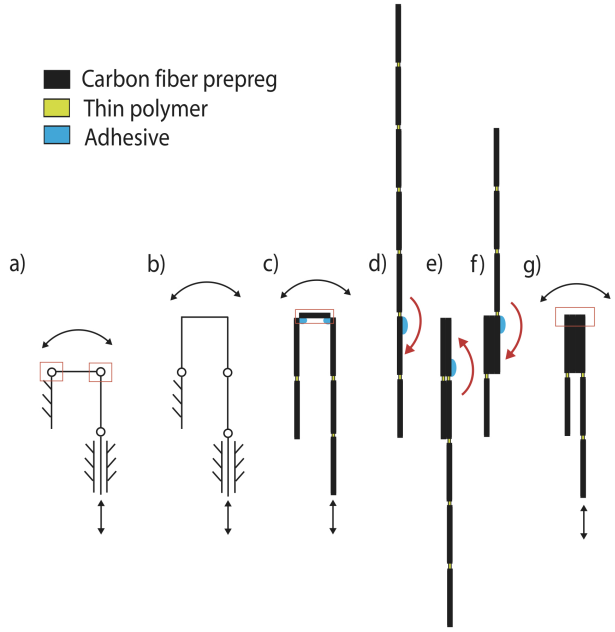

Fig. 9 To facilitate folding of the (a)-(b) transmission as an alternative to (c) two 90 degree folds, (d)-(g) three 180 degree folds are used.

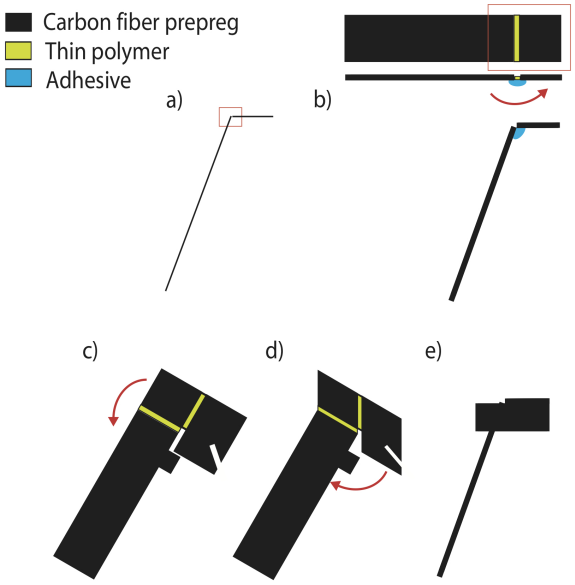

Fig. 10 (a)-(b) To create accurate folds for the leg, which is to be angled outwards, (c)-(e) notches and tabs are used for alignment.

posite adheres the flex circuits to the actuators. In the same step, the actuator mount is bonded to the actuators also using a machined composite prepreg layered between the actuators and actuator mount. The circuits connect the grounds for each actuator in one segment as well as the high voltage signals. This requires a flex circuit that connects the bottom piezoelectric plates on one side of each actuator to the top plates of the opposite side of the actuators. To mimic double sided flex circuits, two traces are soldered to the main flex circuit and bonded to the tops of the actuators. Wires are soldered to the bond pads for each signal and connected to pins that interface with the external power supply and controller. The flex circuits bonded to actuators are shown in Fig. 11 before being folded into the 3D segment. This figure shows the copper traces connected to the actuators. The small squares on the tops of each actuator are the composite prepreg squares placed on the backside of each bond pad and cured to the actuator. These traces and facing down in the figure, while the traces wrapping around to the opposite side of the actuator are facing upwards and bonded to the actuator in the same way.

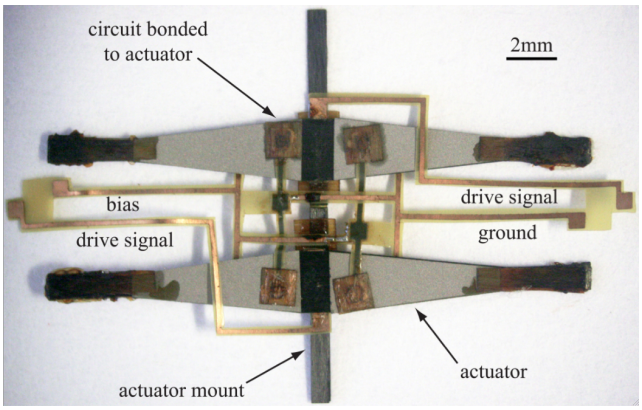

Fig. 11 The internal circuitry of one segment involves bonding custom fabricated copper traces to the actuators. The actuators for one segment have traces connecting grounds and high voltage signals of each actuator.

Upon bonding the actuators to the flex circuits, the actuators are folded perpendicular to each other using the attached actuator mount to rigidly hold them in place. Two transmissions and two legs are glued to each segment, and the segment is then adhered to the folded backbone. This last step is done using a thermoplastic, which allows a broken segment to easily be removed by heating the bond to the backbone and releasing the solder connections. Finally, the feet, laser-machined from 3 layers of pre-cured carbon fiber composite and coming to a sharp point to facilitate rotation of the feet with respect to ground, are glued to the legs. The completed three segment robot used to obtain the experimental results presented in Sect. 5 is shown in Fig. 12.

5 EXPERIMENTAL RESULTS

The experimental setup used to control and analyze the motion of the robot includes an xPC target system

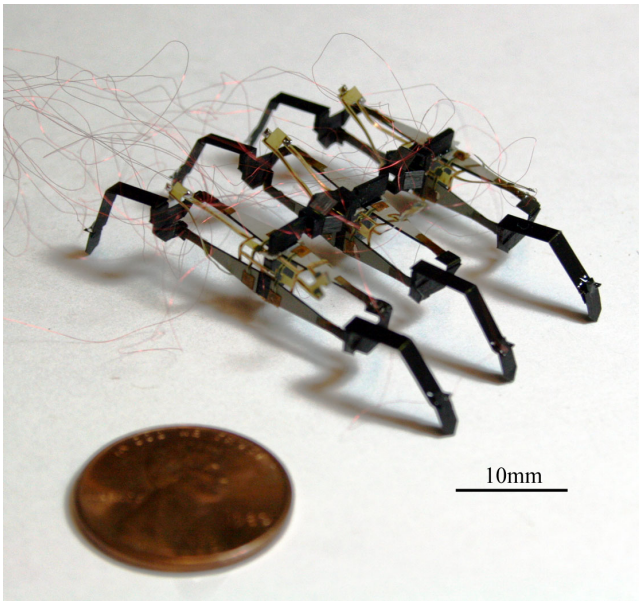

Fig. 12 Assembled three-segment centipede microrobot.

(Mathworks), which sends the appropriate drive signals to a custom-built 20-channel high-voltage amplifier via a D/A board. 50 μm diameter wires are used to connect the microrobot to the external power supply and controller and have minimal interference with the motion of the robot. A sinusoidal drive signal with an amplitude of 200 V is used to control the torque applied at the shoulder joint in the horizontal plane and the rotation of the swing leg. While this is not necessarily the optimal control, it results in forward locomotion. Stance control utilizes a signal ramped between ground and the bias voltage of the actuators as it is desirable to have the feet switch instantaneously; however, the brittle nature of the actuators does not allow a square wave to be used. The stance and swing feet switch orientation at the peak of the sinusoidal horizontal plane motion drive signal to allow the correct torque to be applied to the stance foot and the swing foot to reset in preparation for the next step.

The microrobot walks on a flat surface, and the motion is captured at 30 fps using a Pixelink camera. Forward straight-line locomotion was successful and frames from the motion of the microrobot walking with a 2 Hz sinusoidal drive signal are shown in Fig. 13. ProAnalyst motion tracking software was used to track critical points on the robot, and the leg and body angles were extracted. The experimental leg and body angles for the middle segment are plotted with those predicted by the dynamic model using the experimental parameters in Fig. 14. The drive signal for the simulation is also plotted. As can be seen, the experimental and theoretical values match closely, proving the effectiveness of the dynamic model. Variations in the motion could be due to a slight coupling between the horizontal and vertical plane motion due to the fact that the feet switching is not instantaneous. The drive signal for the stance control is not a perfect square wave, but instead is ramped between the two limits, as an instantaneous change in voltage will damage the piezoelectric actuator. This means that the stance change is not quite instantaneous as assumed in the model, which causes the timing difference shown in the figure. The stance begins to change before the horizontal plane motion actuators reverse direction. Additionally, the difference between the predicted and actual leg angle could be due to this slight coupling between the vertical and horizontal plane motion, which is not included in the model. Walking with a 2 Hz drive signal results in forward motion of the robot of about 1 body length in 10 seconds, with a step size between 0.75 and 1 mm. The step size is dependent on the gait and is expected to vary with different body undulations. Future work will focus on more locomotion studies at increased speeds using higher frequency drive signals made possible by the high bandwidth of the piezoelectric actuators.

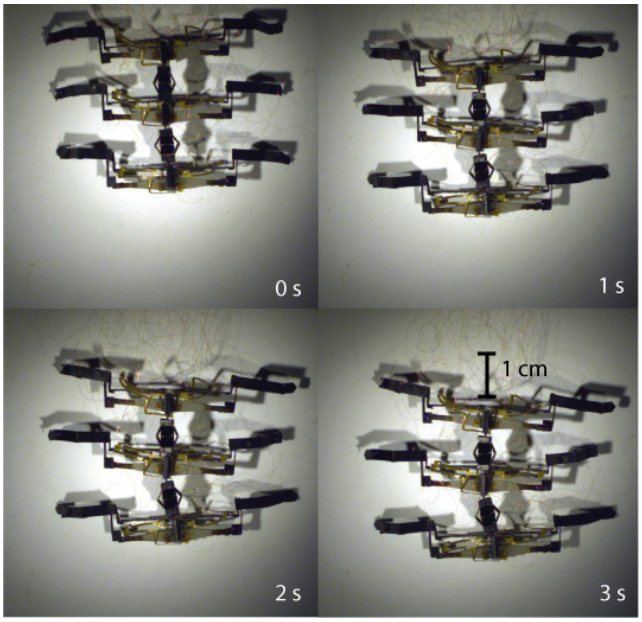

Fig. 13 Frames of motion of three-segment centipede microrobot. See supplemental information for video of robot.

6 CONCLUSIONS AND FUTURE WORK

The design, detailed dynamic model, and fabrication of a three-segment ambulatory microrobot with a flexible backbone was presented. Forward locomotion was

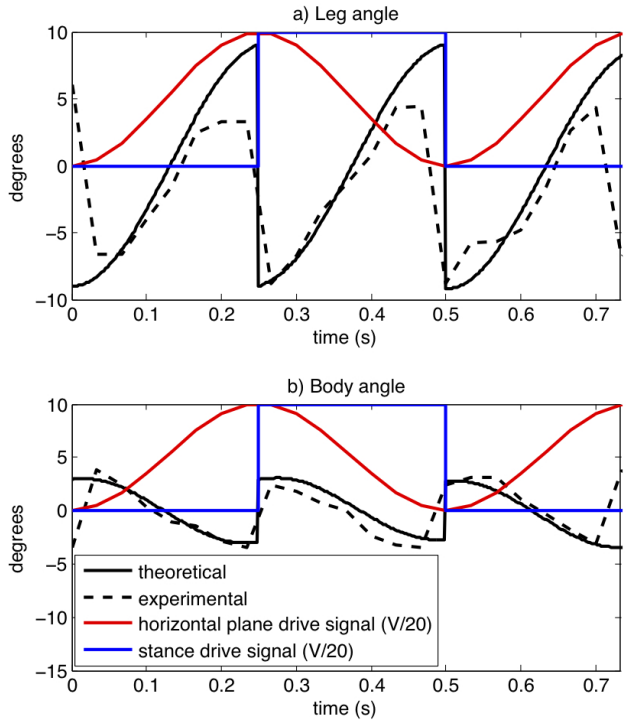

Fig. 14 Theoretical and experimental a) leg and b) body angles for middle segment of three-segment robot plotted with simulation drive signals for three steps.

demonstrated. The generality of the dynamic model and modular design of the microrobot lends itself to easily be expanded to create a microrobot with more segments which is the focus of current work. Robustness studies can be performed both in simulation and experimentally to determine the optimal number of legs for an ambulatory microrobot, having a significant impact pertaining to the design of successful ambulatory microrobots and terrestrial robots at larger scales and enhancing the understanding of legged locomotion of biological creatures and perhaps the evolutionary pressures that lead to a particular number of legs. Varying the phase difference of the drive signal between different segments can create different gaits and a more in depth study of control techniques for many-legged ambulatory robots can be performed.

The dynamic model will be expanded to include turning to add more versatility to the types of maneuvers this robot is able to perform, and the model will be used as a feed-forward controller. Additional control schemes utilizing the undulatory modes of the robot to enhance locomotion will be developed and tested. The dynamic model can be expanded to include actuated degrees of freedom in the backbone in both the horizontal and vertical planes. Climbing vertical surfaces and inclines is also a goal of this microrobot. While the dynamic model for the horizontal plane motion presented here is useful for optimization and control on horizontal surfaces, a vertical plane model and experimental measurements of ground forces could assist in climbing and the design of adhesive mechanisms.

The integrated flex circuits were a major milestone in the batch fabrication techniques associated with many-legged ambulatory microrobots; however, additional batch fabrication methods are desired to further automate the construction of microrobots. The modular, repeated segments that make up this robot allow it to be the ideal platform for inspiring batch fabrication. An onboard controller and power source will also be added to each segment, following work on small-scale electronics presented in (Karpelson et al 2009).

While this microrobot serves as inspiration for research related to fabrication, control, climbing, and modeling, once autonomous, it also has the ability to be used for distributed robotics applications, search and rescue missions, hazardous environment exploration, and surveillance.

Acknowledgements This work was partially supported by the National Science Foundation (under award number IIS-0811571). Any opinions, findings and conclusions or recommendations expressed in this material are those of the authors and do not necessarily reflect those of the National Science Foundation. This research was also made with Government support under and awarded by DoD, Air Force Office of Scientific Research, National Defense Science and Engineering Graduate (NDSEG) Fellowship, 32 CFR 168a.

References

Baisch A, Wood R (2009) Design and fabrication of the harvard ambulatory microrobot. 14th Int Symp of Robotics Research

Birkmeyer P, Peterson K, Fearing R (2009) DASH: A Dynamic 16g Hexapedal Robot. Proc IEEE/RSJ International Conference on Intelligent Robots and Systems

Chen V, Tedrake R (2007) Passive dynamic walking with knees: a point foot model. Massachusetts Institute of Technology

Edgecombe G, Giribet G (2006) Evolutionary biology of centipedes (Myriapoda: Chilopoda). The Annual Review of Entomology 52:151–170

Full R, Tu M (1991) Mechanics of a rapid running insect: two-, four- and six-legged locomotion. Journal of Experimental Biology 156:215–231

Hoffman K, Wood R (2010) Towards a multi-segment ambulatory microrobot. Proc IEEE International Conference on Robotics and Automation

Holmes P, Full R, Koditschek D, Guckenheimer J (2006) The dynamics of legged locomotion: Models, analyses, and challenges. Dynamics 48(2):207–304

Hoover A, Steltz E, Fearing R (2008) RoACH: An autonomous 2.4 g crawling hexapod robot. IEEE/RSJ International Conference on Intelligent Robots and Systems pp 26–33

Jimenez B, Ikspeert A (2007) Centipede Robot Locomotion

Karpelson M, Wei GY, Wood R (2009) Milligram-scale high-voltage power electronics for piezoelectric microrobots. IEEE International Conference on Robotics and Automation

Lobontiu N, Goldfarb M, Garcia E (2001) A piezoelectric-driven inchworm locomotion device. Mechanism and Machine Theory 36(4):425–443

Manton S, Harding M (1952) The evolution of Arthropodan locomotory mechanisms - Part 3. The locomotion of the Chilopoda and Pauropoda. Journal of the Linnean Society of London, Zoology 42(284):118–167

Matthey L, Righetti L, Ijspeert A (2008) Experimental study of limit cycle and chaotic controllers for the locomotion of centipede robots. IEEE/RSJ International Conference on Intelligent Robots and Systems pp 1860–1865

Nohara B, Nishizawa T (2005) An Optimal Working Function Based on the Energetic Cost for Myriapod Robot Systems: How Many Legs Are Optimal for a Centipede? Journal of Vibration and Control 11(10):1235

Sahai R, Avadhanula S, Groff R, Steltz E, Wood R, Fearing R (2006) Towards a 3g Crawling Robot through the Integration of Microrobot Technologies. Proc IEEE International Conference on Robotics and Automation

Sfakiotakis M, Tsakiris D (2009) Undulatory and pedundulatory robotic locomotion via direct and retrograde body waves. IEEE International Conference on Robotics and Automation pp 3457–3463

Steltz E, Seeman M, Avadhanula S, Fearing R (2006) Power electronics design choice for piezoelectric microrobots. In: IEEE/RSJ International Conference on Intelligent Robots and Systems, pp 1322–1328

Wood R, Steltz E, Fearing R (2005) Optimal energy density piezoelectric bending actuators. Sensors & Actuators: A Physical 119(2):476–488

Wood R, Avadhanula S, Sahai R, Steltz E, Fearing R (2008) Microrobot design using fiber reinforced composites. Journal of Mechanical Design 130(5):052,304